Available online at www.sciencedirect.com
ScienceDirect
Journal of Computational Physics 227 (2007) 513–536
JOURNAL OF COMPUTATIONAL PHYSICS
www.elsevier.com/locate/jcp

The effect of the 2-D Laplacian operator approximation on the performance of finite-difference time-domain schemes for Maxwell's equations

Anastasios H. Panaretos *, James T. Aberle, Rodolfo E. Díaz

Department of Electrical Engineering, Arizona State University, Tempe, AZ 85287-8406, USA

Received 4 December 2006; received in revised form 31 July 2007; accepted 2 August 2007
Available online 4 September 2007

Abstract

The behavior of the finite-difference time-domain method (FDTD) is investigated with respect to the approximation of the two-dimensional Laplacian, associated with the curl–curl operator. Our analysis begins from the observation that in a two-dimensional space the Yee algorithm approximates the Laplacian operator via a strongly anisotropic 5-point approximation. It is demonstrated that with the aid of a transversely extended-curl operator any 9-point Laplacian can be mapped onto FDTD update equations. Our analysis shows that the mapping of an isotropic Laplacian approximation results in an isotropic and less dispersive FDTD scheme. The properties of the extended curl are further explored and it is proved that a unity Courant number can be achieved without the resulting scheme suffering from grid decoupling. Additionally, the case of a 25-point isotropic Laplacian is examined and it is shown that the corresponding scheme is fourth order accurate in space and exhibits isotropy up to sixth order. Representative numerical simulations are performed that validate the theoretically derived results.

Keywords: Finite-difference time-domain method; Laplacian operator; Curl operator; Electromagnetics

1. Introduction

The Yee algorithm is undoubtedly one of the most popular finite-difference (FDTD) approximations to Maxwell's equations, mainly due to its conceptual simplicity and ease of implementation. Its main characteristic is that Maxwell's equations are treated in a coupled curl form, and in a leapfrog time-stepping manner. In addition the involved first order partial derivatives are approximated via second order accurate central finite differences, on a staggered spatio-temporal grid arrangement. Yet, the scheme suffers from numerical dispersion as well as phase velocity anisotropy. Their deteriorating effects become very pronounced when the problems under study involve long integration times or results are required over a wide frequency range.

* Corresponding author.
E-mail address: tassos@asu.edu (A.H. Panaretos).

0021-9991/$ - see front matter © 2007 Elsevier Inc. All rights reserved.
doi:10.1016/j.jcp.2007.08.019

Obviously, the naive approach to mitigate the effects of these drawbacks is to use finer grids, however this is not always feasible due to the increase of computational cost.

The inherent dispersion and anisotropy errors of the Yee algorithm have so far stimulated a great research effort towards the development of improved FDTD schemes. The latter can be viewed as different flavors of the Yee algorithm since they retain many of its characteristics. The reasonable trend in order to tackle the dispersion and anisotropy errors is to employ higher order approximation to the first order partial derivatives. This path has been successfully followed by many researchers. Selectively we mention the work of Fang in [1] and Yefet and Petropoulos in [2], where second order accurate in time and fourth order accurate in space schemes were presented. Along similar lines Zygiridis and Tsiboukis in [3] as well as Sun and Trueman in [4] optimized versions of the Fang scheme were derived by appropriately modifying the weights of the spatial derivatives' approximation. Also Hadi and Piket-May in [5] proposed an improved (2,4) scheme by applying Ampere's law on several loops. An alternative formulation is the one presented by Young et al. in [6]. The proposed scheme combined compact finite differences [7] for the spatial derivatives, with a Runge–Kutta integrator for time advancement. Of particular interest are those FDTD schemes developed on hexagonal grids, such as the one presented by Liu in [8] and recently by Xiao et al. in [9], which exhibit superior isotropy characteristics and reduced dispersion errors. Furthermore, in [10] dispersion error reduction was achieved by introducing artificial anisotropy in the regular FDTD update equations. This can be done through appropriate modification of the constitutive parameters of the modeled material. The material properties can be tuned and dispersion characteristics can be optimized with respect to a single frequency. Finally Wang and Teixeira in a series of papers [11–15] gave an elaborate analysis on how to eliminate the dispersion error over a certain frequency bandwidth or a particular angular span. Note that a detailed comparison of several low-dispersion schemes can be found in [16], while a very informative listing of past and current trends in FDTD improvement can be found in [17]. Another low-dispersion time-domain scheme is the pseudo-spectral time-domain (PSTD) method pioneered in the area of electromagnetics by Liu [18,19] and still being expanded and refined [20]. A very detailed overview of higher order time-domain methods has been given by Hesthaven in [21]. Finally, Kantartzis and Tsiboukis in [22] have given an exhaustive and mathematically elaborate description of higher order FDTD schemes. This work includes a collection of the authors' contributions in the field, such as [23,24], as well as an overview of general higher order FDTD strategies.

Our approach is motivated by the fact that Maxwell's equations essentially propagate electromagnetic waves through the curl–curl operator, whose fundamental element is the two-dimensional transverse Laplacian operator. Unfortunately, since FDTD works with Maxwell's equations in individual curl form, the existence of this term is masked and hence its importance can be easily neglected. This is further supported by the fact that the Yee algorithm, during a time-step, indirectly approximates the "hidden" Laplacian term via a strongly anisotropic 5-point representation. As lucidly demonstrated in Section 2 this is solely responsible for the scheme's poor isotropy performance. Consequently, its amelioration is likely if the Laplacian term is approximated more accurately. Obviously since the direct mapping of a Laplacian approximation into FDTD updating is impossible, the goal is to improve the curl operator in FDTD in such a way that it yields indirectly a "good" and "as isotropic as possible" transverse Laplacian. The derivation presented here thus starts from a transverse Laplacian that is best seen in a homogeneous isotropic space; but the final result, more effective curl operators, then can be applied in the arbitrary anisotropic, inhomogeneous case. Similarly, for clarity and simplicity a 2-D space is treated but the application to 3-D is direct as evidenced in [25].

The development presented here will proceed as follows: In Section 3 it is shown that in a 2-D space only the curl operator that lies on the same plane with the transverse Laplacian needs to be modified resulting on what we refer to as the extended-curl operator. As further demonstrated in Section 3 the latter allows mapping of any 9-point Laplacian onto FDTD update equations. The scheme that corresponds to the most isotropic 9-point Laplacian is shown to be characterized by superior isotropy, less dispersion and a higher Courant number. Moreover, further experimentation with the extended-curl schemes reveals that a unity Courant number can be supported (Section 5). As a matter of fact there is an infinite number of extended-curl realizations that exhibit this feature. Finally in Section 8 it is shown how this formalism can be extended to the case of a 25-point isotropic Laplacian, resulting in a "hyper-isotropic" scheme. As a final comment it should be mentioned that our approach should not be confused with those that approximate the 2-D and 3-D Maxwell's equations with the 2-D and 3-D scalar wave equations, respectively. This is better justified from the 3-D formulation of our

method, where the extended-curl operators are defined with respect to the 3 transverse 2-D Laplacians and not by the 3-D one [25]. Also it should be noted that throughout this document the second order accurate leapfrog scheme is adopted for time integration.

2. Motivation

The approach presented herein stems from the fact that Maxwell's equations, in the case of a linear, isotropic, and homogeneous medium, propagate electromagnetic waves essentially through the curl–curl ($\nabla\times\nabla\times$) operator as seen in the well-known vector wave equation:

$$\nabla\times\nabla\times\mathbf{E} = -\mu\varepsilon\partial_{tt}^2\mathbf{E} \tag{1}$$

In the general case of a divergenceless field, the curl–curl operator can be separated explicitly into a transverse Laplacian and cross terms. For instance, taking the z-component of (1) we have

$$-\mu\varepsilon\partial_{tt}^2 E_z = (\nabla\times\nabla\times\mathbf{E})_z = \partial_z(\partial_x E_x + \partial_y E_y) - \nabla_{xy}^2 E_z \tag{2}$$

It can be seen that the right hand side of (2) consists of two terms, one of which is a 2-D Laplacian, transverse to the direction of the component under consideration. Therefore, it can be concluded that the 2-D Laplacian is a fundamental element of the 3-D curl–curl operator, or that the 2-D Laplacian is implicit in the two successive curl operations.

Here, we consider a two-dimensional space and a transverse, with respect to z, electric (TE_z) field polarization. (The same analysis can be carried out for the TM_z case as well.) For the 2-D TE_z case, the time-domain Maxwell's equations are given by

$$\partial_t H_z = \frac{1}{\mu}(\partial_y E_x - \partial_x E_y) \tag{3}$$

$$\partial_t E_x = \frac{1}{\varepsilon}\partial_y H_z \tag{4}$$

$$\partial_t E_y = -\frac{1}{\varepsilon}\partial_x H_z \tag{5}$$

The most popular discrete approximation to this set of equations is the finite-difference time-domain (FDTD) method introduced by Yee [26], and later expanded and refined by various researchers [27,28]. The method assumes a staggered field arrangement both in space and time; it employs second order accurate central finite differences for the approximation of spatial derivatives, and the leapfrog scheme for time integration. The corresponding equations comprise what is referred to as the "Yee-scheme" or "conventional FDTD", and they are given by

$$\delta_t H_z\big|_{i+\frac{1}{2},j+\frac{1}{2}}^{n+\frac{1}{2}} = \frac{1}{\mu}\left(\delta_y E_x\big|_{i+\frac{1}{2},j+\frac{1}{2}}^{n+\frac{1}{2}} - \delta_x E_y\big|_{i+\frac{1}{2},j+\frac{1}{2}}^{n+\frac{1}{2}}\right) \tag{6}$$

$$\delta_t E_x\big|_{i+\frac{1}{2},j}^{n} = \frac{1}{\varepsilon}\delta_y H_z\Big|_{i+\frac{1}{2},j}^{n} \tag{7}$$

$$\delta_t E_y\big|_{i,j+\frac{1}{2}}^{n} = -\frac{1}{\varepsilon}\delta_x H_z\Big|_{i,j+\frac{1}{2}}^{n} \tag{8}$$

where

$$\delta_x u_i = \frac{u_{i+\frac{1}{2}} - u_{i-\frac{1}{2}}}{\Delta x} \quad \text{and} \quad \delta_t u^n = \frac{u^{n+\frac{1}{2}} - u^{n-\frac{1}{2}}}{\Delta t} \tag{9}$$

Due to the two-stage "time-marching" nature of the leapfrog scheme, Eqs. (6)–(8) are referred to as the "FDTD update equations" for conventional FDTD. Notice that in this formulation Maxwell's equations are treated as a first order system of two coupled curl equations. Evidently, the existence of the Laplacian term is masked, meaning that the latter is not directly computed during an FDTD calculation. Conceptually, the indirect generation of the Laplacian approximation means that the Yee-scheme Laplacian results by default and not by purposeful choice. In what follows the accuracy of this approximation is examined.

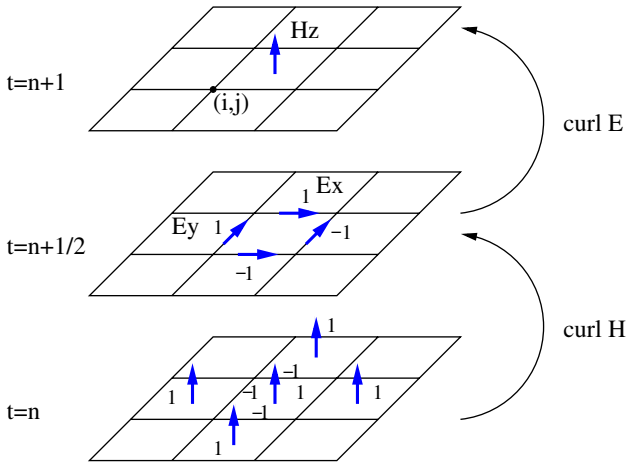

Fig. 1. Curl–curl approximation in the Yee-scheme.

Hence, let us examine the updating sequence during a time-step that leads to the computation of the H_z component. Notice that for this field mode, $(\nabla\times\nabla\times)_z$ reduces to ∇^2_{xy}, since it has been assumed that there is no variation along the z-direction. In order to get a better insight into the above scenario, consider the graphical representation in Fig. 1. The FDTD formalism dictates that the value of $H_z\left(i+\frac{1}{2},j+\frac{1}{2}\right)$ at the $(n+1)$th time-step is obtained as a sequence of two curl operations, performed on magnetic and electric fields, respectively. Referring to Fig. 1 and going backwards in time, we see that $H_z\left(i+\frac{1}{2},j+\frac{1}{2}\right)$ is computed as a weighted sum of four curling electric field components. This is because conventional FDTD approximates the curl operator component $(\nabla\times\mathbf{E})_z$ through a 4-point discretization. In the same fashion, these electric field components are computed by two curling magnetic field components (not four since it has been assumed no variation along the z-direction) at time-step n, with the one located at the center contributing four times in total. Therefore, we can see that the variation of $H_z\left(i+\frac{1}{2},j+\frac{1}{2}\right)$ within a time-step is determined by its spatial variation represented by a 2-D Laplacian, transverse to its direction (z), where the Laplacian is approximated as

$$\nabla^2_{xy}H_z\left(i+\frac{1}{2},j+\frac{1}{2}\right)\sim -4H_z\left(i+\frac{1}{2},j+\frac{1}{2}\right)+H_z\left(i+\frac{3}{2},j+\frac{1}{2}\right)+H_z\left(i-\frac{1}{2},j+\frac{1}{2}\right)+H_z\left(i+\frac{1}{2},j+\frac{3}{2}\right)+H_z\left(i+\frac{1}{2},j-\frac{1}{2}\right) \tag{10}$$

Accordingly, it can be concluded that the 4-point curl discretization performed by the Yee-scheme results in the strongly anisotropic 5-point Laplacian approximation given by

$$\nabla^2 u_{i,j}=\frac{1}{h^2}\left[-4u_{i,j}+(u_{i+1,j}+u_{i-1,j}+u_{i,j+1}+u_{i,j-1})\right]-\frac{h^2}{12}\left(\partial_x^4+\partial_y^4\right)u_{i,j}+\mathcal{O}(h^4) \tag{11}$$

where h is the spatial increment. The strong anisotropy of (11) is due to its leading error term (LET); it exhibits dispersion properties dependent on the propagation angle, and consequently introduces dispersion error anisotropically in the computational domain. Given the above, it is intuitively expected that superior FDTD accuracy could be achieved if a more accurate Laplacian representation was employed. In what follows, first a more accurate version of the discrete Laplacian is presented. Afterwards, it is demonstrated how the update equations should be modified, so that the more accurate Laplacian representation is utilized.

3. Formulation

The approximation in (11) is a member of the family of 9-point Laplacian approximations whose general form is given by [29,30]

$$\nabla^2 u_{ij} \approx c_0 u_{i,j} + c_1(u_{i+1,j} + u_{i-1,j} + u_{i,j+1} + u_{i,j-1}) + c_2(u_{i+1,j+1} + u_{i+1,j-1} + u_{i-1,j-1} + u_{i-1,j+1}) \tag{12}$$

where c_0, c_1 and c_2 are properly chosen coefficients. It is easy to verify that the highest accuracy that can be achieved from (12) is second order. However by judiciously choosing c_0, c_1 and c_2 one can obtain the following Laplacian approximation:

$$\nabla^2 u_{i,j} = \frac{1}{6h^2}[-20u_{i,j} + 4(u_{i+1,j} + u_{i-1,j} + u_{i,j+1} + u_{i,j-1}) + (u_{i+1,j+1} + u_{i+1,j-1} + u_{i-1,j-1} + u_{i-1,j+1})] - \frac{h^2}{12}\nabla^4 u_{i,j} + \mathcal{O}(h^4) \tag{13}$$

In particular the derivation of the above requires us to first perform a 2-D Taylor expansion on (12). Then c_0, c_1 and c_2 are subjected to appropriately chosen conditions so that second order of accuracy is obtained, and the corresponding LET turns out to be the biharmonic operator, which yields a 4th order isotropic approximation.

For the 9-point Laplacians' family, the combination of c_0, c_1 and c_2 that yields the biharmonic operator is unique. Moreover, the latter is the highest degree of isotropy that can be achieved. If a higher degree of isotropy is required then widened Laplacian stencils must be employed. This will be further elaborated later in this paper.

Let us now determine how to modify the update equations so that the 9-point Laplacian of (13) is indirectly computed. Recall that the ultimate objective is to modify the update equations so that the value of any H_z component at any time-step is determined by nine appropriately weighted H_z components from the previous time-step. First the update equations' stencil needs to be chosen so that a 9-point Laplacian stencil is retrieved. There are two ways to achieve the above and these are depicted in Fig. 2(a) and (b).

The first approach [Fig. 2(a)] is to retain a 4-point discretization, like the Yee-scheme suggests, for the curl operation that results to an H_z component update. However, for the update of E_x and E_y a *flux-averaging* strategy is required in order to "reach out" for the diagonally located H_z's. With respect to Fig. 2(a) it can be seen that the E_y component depicted by the thick arrow is updated not only by the immediately neighboring H_z components, but also by the ones defining the flux in the upper and lower cells, with respect to the updated component's vector direction (also shown thick).

The second approach is shown in Fig. 2(b). In this case a complementary strategy is adopted: for the updating of both the E_x and E_y components only the immediately neighboring H_z's are used, similar to what the Yee-scheme suggests. However, we modify the curl approximation that lies on the same plane on which the Laplacian is defined (for this problem the x–y plane). This modification suggests that the curl operator that

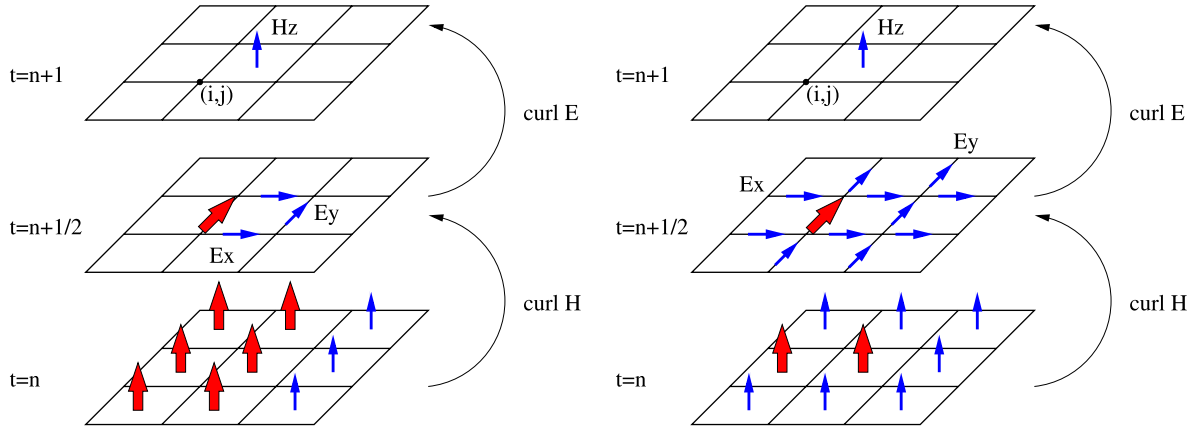

(a) Flux averaging approach. (b) Extended-curl approach.

Fig. 2. Update equations' modification for a 9-point Laplacian representation. The thick arrows indicate curl-related components between the first half time-step.

results in an H_z component update be longitudinally extended. Essentially this is a longitudinal extension of the curl-related derivatives, with respect to the direction of the derived component, and it will be referred to as the *extended-curl* operator.

The choice between the two approaches is made based upon their ability to provide physically meaningful results. First of all, one notices that for this TE_z field configuration the magnetic Gauss' law is exactly satisfied since

$$\partial_t \nabla \cdot (\mu \mathbf{H}) = \partial_t (\partial_x, \partial_y, 0) \cdot (0, 0, \mu H_z) = 0 \tag{14}$$

The above suggests that no matter how the H_z update equation is modified in this 2-D space, magnetic flux conservation is always satisfied. In contrast, the modification of the electric field components update equations is more restricted since it is not always guaranteed that electric flux is preserved. Hence it becomes apparent that retaining the Yee algorithm update equations for E_x and E_y, is a very convenient and accurate "tactic" since the electric flux conservation is automatically satisfied [27], i.e.

$$\delta_t \left(\delta_x D_x|_{i,j}^n + \delta_y D_y|_{i,j}^n \right) = 0 \tag{15}$$

which is the discretised version of the electric Gauss' Law, i.e.

$$\partial_t \nabla \cdot (\varepsilon \mathbf{E}) = 0 \tag{16}$$

Bearing this in mind, it is obvious that the flux-averaging approach does not comply with the above scenario. In particular, electric flux is not conserved and consequently its implementation will provide with solutions infested by spurious solutions. In contrast, the extended-curl approach is in absolute agreement with both of the Gauss' laws. Accordingly, this approach is followed for the development of our scheme.

To complete the determination of the extended-curl operator its weights need to be specified. From the previous discussion the updating equation for H_z is given by

$$\delta_t H_z|_{i+\frac{1}{2},j+\frac{1}{2}}^{n+\frac{1}{2}} = \frac{1}{\mu} \left[\beta \left(\delta_y E_x|_{i+\frac{3}{2},j+\frac{1}{2}}^{n+\frac{1}{2}} - \delta_x E_y|_{i+\frac{1}{2},j+\frac{3}{2}}^{n+\frac{1}{2}} \right) + \alpha \left(\delta_y E_x|_{i+\frac{1}{2},j+\frac{1}{2}}^{n+\frac{1}{2}} - \delta_x E_y|_{i+\frac{1}{2},j+\frac{1}{2}}^{n+\frac{1}{2}} \right) + \beta \left(\delta_y E_x|_{i-\frac{1}{2},j+\frac{1}{2}}^{n+\frac{1}{2}} - \delta_x E_y|_{i+\frac{1}{2},j-\frac{1}{2}}^{n+\frac{1}{2}} \right) \right] \tag{17}$$

where α and β are arbitrary real numbers. Recall that for E_x and E_y, we resort to the standard update equations, that is (7) and (8). Now, if we apply the sequence of these update equations for a time-step cycle as depicted in Fig. 2(b), then the resulting Laplacian approximation of any H_z component is given by

$$\nabla^2 u_{ij} \approx \frac{1}{h^2} [-4\alpha u_{i,j} + (\alpha - 2\beta)(u_{i+1,j} + u_{i-1,j} + u_{i,j+1} + u_{i,j-1}) + 2\beta(u_{i+1,j+1} + u_{i+1,j-1} + u_{i-1,j-1} + u_{i-1,j+1})] \tag{18}$$

where $u_{ij} \equiv H_z(i + \frac{1}{2}, j + \frac{1}{2})$. The values of α and β for any desired Laplacian approximation are given by equating like terms in (18) and (12). For instance (13) corresponds to the following extended-curl weights:

$$\left.\begin{array}{l} -4\alpha = -20/6 \\ 2\beta = 1/6 \\ a - 2\beta = 4/6 \end{array}\right\} \Rightarrow \begin{array}{l} \alpha = 5/6 \\ \beta = 1/12 \\ \alpha - 2\beta = 4/6 \end{array}$$

where obviously the third equation is satisfied by the calculated values for α and β.

4. Stability and dispersion analysis

Let us consider first the scheme that corresponds to (13), that is the extended-curl operator weighted with $\alpha = 5/6$ and $\beta = 1/12$. In order to investigate the proposed scheme's stability, a 2-D unbounded, linear and homogeneous space is assumed. The time-step bound that ensures stability can be obtained by employing a standard von Neumann analysis. This requires that spatial discrete Fourier modes of the form

$$u_{i,j}^n = \hat{u}^n(\tilde{k}_x, \tilde{k}_y) \mathrm{e}^{-\mathrm{j}(\tilde{k}_x i \Delta x + \tilde{k}_y j \Delta y)} \tag{19}$$

are substituted into the update equations (7), (8) and (17). $\tilde{k}$ denotes the discrete wavenumber which, for an ideal FDTD algorithm, should be equal to the physical wavenumber, $k = \omega/c$. The resulting equations can be cast into the following matrix form:

$$\hat{\mathbf{u}}^{n+1} = \mathbf{G}\hat{\mathbf{u}}^{n} \tag{20}$$

where $\hat{\mathbf{u}}^n = \left[\widehat{E}_x^{n+\frac{1}{2}}\ \widehat{E}_y^{n+\frac{1}{2}}\ \widehat{H}_z^{n}\right]^{\mathrm{T}}$ is the field component vector, $\mathbf{G}$ is the amplification matrix given in (21)

$$\mathbf{G} = \begin{pmatrix} 1 & 0 & 2\mathrm{j}\xi_y S_y \\ 0 & 1 & -2\mathrm{j}\xi_x S_x \\ 2\mathrm{j}\zeta_y S_y & -2\mathrm{j}\zeta_x S_x & 1 - 4\xi_y\zeta_y S_y^2 C_x - 4\xi_x\zeta_x S_x^2 C_y \end{pmatrix} \tag{21}$$

Also, $\xi_w = \Delta t/\varepsilon\Delta w$, $\zeta_w = \Delta t/\mu\Delta w$, $S_w = \sin(\tilde{k}_w\Delta w/2)$, $C_w = \alpha + 2\beta\cos(\tilde{k}_w\Delta w)$ with $w \in \{x, y\}$. The eigenvalues of the amplification matrix are the following:

$$\lambda_1 = 1, \quad \lambda_{2,3} = 1 - 2\Psi \pm 2\sqrt{-\Psi + \Psi^2} \tag{22}$$

where $\Psi = \xi_x\zeta_x S_x^2 C_y + \xi_y\zeta_y S_y^2 C_x$. The scheme is stable if all eigenvalues lie within the unit circle. This condition is satisfied when the time-step is subjected to the following constraint:

$$\Delta t \leqslant \left(c\sqrt{\frac{S_x^2 C_y}{\Delta x^2} + \frac{S_y^2 C_x}{\Delta y^2}}\right)^{-1} \tag{23}$$

where $c = 1/\sqrt{\varepsilon\mu}$ is the speed of light in the material being modeled. The CFL condition is obtained if in the above inequality we set $\Delta x = \Delta y = h$, and substitute the maximum value of $S_x^2 C_y$ and $S_y^2 C_x$. Thus

$$\Delta t \leqslant \frac{1}{\sqrt{2(\alpha - 2\beta)}}\frac{h}{c} = \frac{\sqrt{3}}{2}\frac{h}{c} \tag{24}$$

where we recall that $\alpha = 5/6$ and $\beta = 1/12$ for our scheme. Notice that if we had chosen $(\alpha, \beta) \equiv (1, 0)$ we would recover the standard FDTD curl, and (24) would yield the Courant limit of the conventional 2-D FDTD scheme, i.e. $S = \sqrt{2}/2$.

The dispersion relation can be derived if we assume discrete temporal Fourier modes in (19), in addition to the spatial ones, or $\hat{u}^n = \hat{u}^0 \mathrm{e}^{\mathrm{j}\omega n\Delta t}$. Hence (20) yields the following eigenvalue problem:

$$\begin{bmatrix} S_t & 0 & -\xi_y S_y \\ 0 & S_t & \xi_x S_x \\ -\zeta_y S_y C_x & \zeta_x S_x C_y & S_t \end{bmatrix} \begin{bmatrix} \widehat{E}_x^0 \\ \widehat{E}_y^0 \\ \widehat{H}_z^0 \end{bmatrix} = \mathbf{0} \tag{25}$$

where $S_t = \sin(\omega\Delta t/2)$. For non-trivial solutions of (25), the determinant of system matrix must be zero. Hence, after some straightforward manipulations, the dispersion relation for the scheme is found to be

$$\left[\frac{1}{c\Delta t}\sin\left(\frac{\omega\Delta t}{2}\right)\right]^2 = \frac{S_x^2 C_y}{\Delta x^2} + \frac{S_y^2 C_x}{\Delta y^2} \tag{26}$$

If we Taylor-expand (26) with respect to both the temporal and spatial variables, the scheme's accuracy can be obtained. Hence we have

$$\left(\frac{\omega}{c}\right)^2 + \mathcal{O}(\Delta t^2) = \tilde{k}_x^2 + \tilde{k}_y^2 - \frac{1}{12}\left[\Delta x^2\tilde{k}_x^4 + \Delta y^2\tilde{k}_y^4 + (\Delta x^2 + \Delta y^2)\tilde{k}_x^2\tilde{k}_y^2\right] + \mathcal{O}(\Delta x^4) + \mathcal{O}(\Delta y^4) \tag{27}$$

Obviously the scheme is second order accurate both in space and time. However, if we write the wavevector in polar form as $(\tilde{k}_x, \tilde{k}_y) = \tilde{k}(\cos\phi, \sin\phi)$ and further assume a uniform discretization, then the spatial LET in (27) yields

$$\mathrm{LET} = h^2\left(\tilde{k}_x^4 + \tilde{k}_y^4 + 2\tilde{k}_x^2\tilde{k}_y^2\right) = h^2\left(\tilde{k}_x^2 + \tilde{k}_y^2\right)^2 = h^2\tilde{k}^4$$

Evidently, the LET in (27) is independent of the propagation angle, meaning that the scheme may be second order accurate but it is fourth order isotropic. Note that for a non-uniform discretization the above result does not hold, since the LET does not complete a perfect square. For comparison purposes, the approximation to the constraint equation obtained by the Yee-scheme is given by (26) if we set $\alpha = 1$, $\beta = 0$ and then Taylor expand. One gets

$$\left(\frac{\omega}{c}\right)^2 + \mathcal{O}(\Delta t^2) = \tilde{k}_x^2 + \tilde{k}_y^2 - \frac{1}{12}\left(\Delta x^2 \tilde{k}_x^4 + \Delta y^2 \tilde{k}_y^4\right) + \mathcal{O}(\Delta x^4) + \mathcal{O}(\Delta y^4) \tag{28}$$

where in this case, the spatial LET strongly depends on the direction of propagation as

$$\mathrm{LET} = h^2\left(\tilde{k}_x^4 + \tilde{k}_y^4\right) = h^2\tilde{k}^4(\cos^4\phi + \sin^4\phi)$$

Also, in the limit of a very fine discretization ($\Delta x \to 0, \Delta y \to 0$), (27) reduces to the constraint equation that governs the propagation of a monochromatic wave in a general 2-D medium. At this point it should be mentioned that the same order of isotropy as the one demonstrated in (27), can be achieved by FDTD implementations on hexagonal grids as has been demonstrated in Liu in [8] and Xiao et al. in [9]. However, the distinct feature of the proposed algorithm is that it retains the simplicity of the Yee-scheme. Thus it is relatively painless to implement existing techniques designed for the Yee-scheme such as absorbing boundary conditions, whereas on a hexagonal grid this is not a trivial task.

5. Extended-curl realizations for a higher Courant number

The preceding analysis revealed that the extended-curl scheme corresponding to the isotropic 9-point Laplacian is characterized by a more relaxed Courant limit, approximately 1.2 times higher than that of the Yee-scheme. In what follows the highest achievable Courant number is investigated, assuming α and β are arbitrary real numbers. More precisely, we are looking for 9-point Laplacian approximations that result in extended-curl schemes with Courant number higher than $S = \sqrt{3}/2$. For reasons that will become clear later in our discussion, let us first examine if a unity Courant number can be achieved. $S = 1$ implies that

$$\Delta t \leqslant \frac{h}{c} \leqslant \frac{1}{\max_{(\alpha,\beta)}\left\{\sqrt{S_x^2 C_y + S_y^2 C_x}\right\}} \frac{h}{c} \tag{29}$$

which leads to the constraint

$$\max_{(\alpha,\beta)}\left\{\sqrt{S_x^2 C_y + S_y^2 C_x}\right\} \leqslant 1 \tag{30}$$

Now, if we Taylor-expand (26) we get

$$\left(\frac{\omega}{c}\right)^2 + \mathcal{O}(\Delta t^2) = (\alpha + 2\beta)\left(\tilde{k}_x^2 + \tilde{k}_y^2\right) + \mathcal{O}(\Delta x^2) + \mathcal{O}(\Delta y^2) \tag{31}$$

The above relation in the limit of a vanishing cell size, should reduce to the constraint equation of a continuous medium, therefore the following condition should hold:

$$\alpha + 2\beta = 1 \tag{32}$$

Given this condition, it is straightforward to show that (Appendix A)

$$\max_{(\alpha,\beta)}\left\{S_x^2 C_y + S_y^2 C_x\right\} = \max_{\beta}\{1, 2 - 8\beta\} \tag{33}$$

If we substitute (33) into (30) and additionally assume that the square rooted quantity must be positive, we get the following constraint:

$$1/8 \leqslant \beta \leqslant 1/4 \tag{34}$$

The system of (32) and (34) can be solved graphically as shown in Fig. 3. The solution pairs lie along the solid line section CD, bounded by the dotted and dashed lines which means that for this continuum of α and β val-

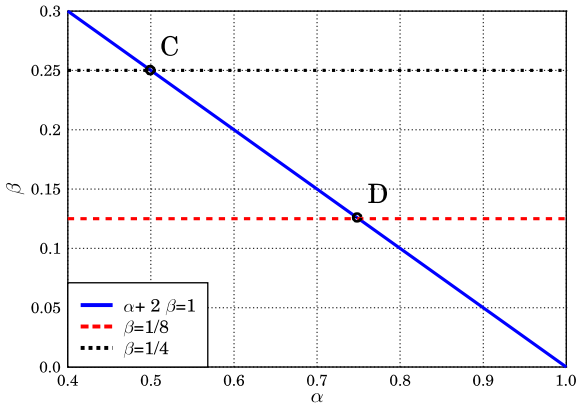

Fig. 3. Determination of parameters α and β.

ues, a Courant number $S = 1$ can be achieved. We refer to this group of extended-curl realizations as the "unity Courant number" schemes. As demonstrated later, there exists an optimum (α, β) pair, determined by the scheme's dispersion properties as well as the scheme's ability to provide accurate results.

Before proceeding to the next section some remarks should be made. First, regarding the generalization of the results presented thus far, we observe that (26) is the numerical dispersion relation that characterizes all members of the extended-curl family including the "unity Courant number" schemes. Similarly, the general time-step bound valid for all extended-curl realizations is the following:

$$\Delta t \leqslant \frac{1}{\sqrt{\max_\beta\{1, 2 - 8\beta\}}} \frac{h}{c} \tag{35}$$

For instance, if $\beta = 0$ the CFL condition for the Yee-scheme is obtained. The above expression reveals that the extended-curl family of schemes cannot support Courant numbers that exceed unity. Clearly, for a Courant number higher than one, the condition $\max_\beta\{1, 2 - 8\beta\} < 1$ should hold, which obviously is impossible.

The last remark can be also justified from the following reasoning. An alternative, although absolutely equivalent, way to interpret the extended-curl schemes is as a combination of two Yee-schemes. As illustrated in Fig. 4 the first one operates on a standard Cartesian grid comprising square cells with size h. The second one exists on a $\pi/4$-rotated Cartesian grid, that consists of rhombic cells with size $h\sqrt{2}$. The two grids are positioned

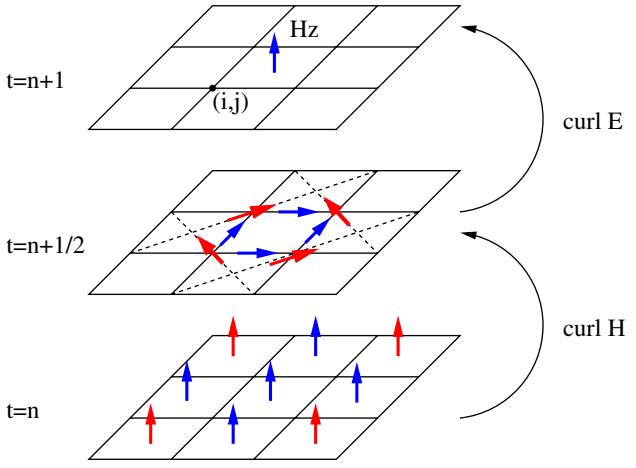

Fig. 4. Alternative extended-curl realization.

so that each square cell of the Cartesian grid is inscribed into a rhombic cell. A rigorous justification of the above is provided by the fact that an alternative representation of (18) is given by [30]

$$\nabla^2 u_{i,j} \approx \frac{\alpha - 2\beta}{h}\left[\left(\frac{u_{i+1,j} - u_{i,j}}{h} - \frac{u_{i,j} - u_{i-1,j}}{h}\right) + \left(\frac{u_{i,j+1} - u_{i,j}}{h} - \frac{u_{i,j} - u_{i,j-1}}{h}\right)\right] + \frac{2\beta}{h\sqrt{2}}\left[\left(\frac{u_{i+1,j+1} - u_{i,j}}{h\sqrt{2}} - \frac{u_{i,j} - u_{i-1,j-1}}{h\sqrt{2}}\right) + \left(\frac{u_{i-1,j+1} - u_{i,j}}{h\sqrt{2}} - \frac{u_{i,j} - u_{i+1,j-1}}{h\sqrt{2}}\right)\right] \tag{36}$$

If we correspond $u_{i,j}$ to $H_z(i+\frac{1}{2}, j+\frac{1}{2})$ then the terms in the first pair of square brackets represent four discrete curl operations which result in four electric field components that lie on the x–y plane, in a closed-loop, circulating formation. These curl operations are performed on a Cartesian grid with cell size h, as indicated by the denominators of the corresponding terms. Regarding the terms in the second pair of square brackets we can conclude that they are a $\pi/4$-rotated version of the first ones, from their corresponding finite-difference stencil. In addition their denominators reveal that the cell size is $h\sqrt{2}$. Consequently, given that the maximum time-step for the Yee-scheme, on a uniform grid is $\Delta t = \frac{h}{c\sqrt{2}}$, then the same time-step for a cell size of $h\sqrt{2}$ becomes $\Delta t = \frac{h}{c}$, which for a uniform Cartesian grid corresponds to a unity Courant number.

It should be mentioned here that Forgy in [31] proposed a scheme that combined a Yee with a staggered collocated grid. Then he expressed the collocated components as an averaging of two adjacent Yee nodes and he derived an equivalent scheme based solely on Yee nodes, which utilizes the extended-curl operator described in this paper. Also, it should be noted that the compatibility between the staggered collocated and the Yee grid, through the above averaging procedure, was first reported by Bi et al. in [32].

6. Anisotropy and dispersion error

In this section the phase velocity isotropy as well the dispersion error of the most interesting extended-curl schemes are examined. These are the Yee-scheme, the most isotropic Laplacian scheme, and two of the unity Courant number schemes, corresponding to points D and C of Fig. 3. Their properties are summarized in Table 1. In order to examine the numerical phase velocity behavior versus propagation angle, it is required to substitute $(\tilde{k}_x, \tilde{k}_y) = \tilde{k}(\cos\phi, \sin\phi)$ in (26), and then to solve iteratively the resulting transcendental equation with respect to the numerical wavenumber $\tilde{k}$. Finally, the numerical phase velocity can be computed as $\tilde{v}_p = \omega/\tilde{k}$.

The corresponding results for a discretization of $\lambda/10$, and using the Courant stability limit are depicted in Fig. 5. There is a strong correlation between the form of the LET shown in the last column of Table 1 and the schemes' isotropy performance. More precisely the bigger the number of cross terms ∂_{xy}^4 by which the LET deviates from the biharmonic operator, the worse the isotropy becomes. The dashed line (Case 2) exhibits highly isotropic phase velocity characteristics corresponding to the most isotropic Laplacian approximation. In the inset figure, there is a more detailed illustration of the phase velocity behavior for this case. It does fluctuate as a function of the propagation angle, however the amplitude of this ripple is of the order of 10^{-4}. Furthermore, the dash-dotted-square-marker line (Case 3) is more isotropic compared to the conventional FDTD scheme of Case 1, but less isotropic than Case 2. Nevertheless, this scheme has the distinguishing characteristic that for propagation along the principal axes ($\phi = 0°, 90°$) the "magic time-step" condition [27,33] is satisfied, meaning that $\Delta t = h/c$ and the dispersion error is totally eliminated for all frequencies. It is interesting to note

Table 1
Comparison of the most representative extended-curl realizations

Case	(α, β)	S	(c_0, c_1, c_2)	LET
(1) Yee-scheme	$(1, 0)$	$\frac{\sqrt{2}}{2}$	$(-4, 1, 0)$	$\nabla^4 - 2\partial_{xy}^4$
(2) The most isotropic Laplacian	$(\frac{5}{6}, \frac{1}{12})$	$\frac{\sqrt{3}}{2}$	$(-\frac{10}{3}, \frac{2}{3}, \frac{1}{6})$	∇^4
(3) Point D in Fig. 3	$(\frac{3}{4}, \frac{1}{8})$	1	$(-3, \frac{1}{2}, \frac{1}{4})$	$\nabla^4 + \partial_{xy}^4$
(4) Point C in Fig. 3	$(\frac{1}{2}, \frac{1}{4})$	1	$(-2, 0, \frac{1}{2})$	$\nabla^4 + 4\partial_{xy}^4$

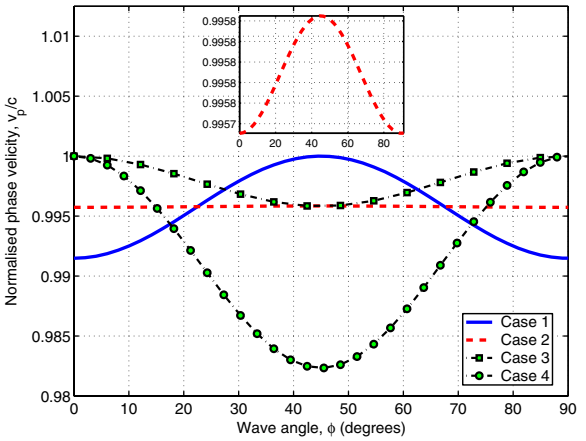

Fig. 5. Normalized phase velocity.

that, the schemes that correspond to Cases 1 and 3 exhibit complementary anisotropy characteristics, with the Case 3 one being overall more isotropic. Finally, Case 4 exhibits the most anisotropic phase velocity, and in particular, the value of the phase velocity minimum at $\phi = 45^\circ$ has been significantly decreased, compare to Case 3. Not only does this severely deteriorate the scheme's isotropy but it also has a detrimental effect on the dispersion error as shown next.

A practical measure of the scheme's performance with respect to the dispersion error reduction is the maximum absolute phase error per wavelength, defined as

$$\psi = 360^\circ \max_{\phi} \left\{ \left| 1 - \frac{\tilde{v}_p}{c} \right| \right\} \tag{37}$$

In Fig. 6 the dispersion error for the four cases is illustrated as a function of the number of cells per wavelength ($N_\lambda = h/\lambda$). Clearly all schemes are second order accurate since the slope of each curve is -2. Moreover, Cases 2 and 3 suffer less from dispersion errors than conventional FDTD. In contrast, Case 4, as expected from the previous analysis, exhibits the worst dispersion characteristics. At this point it can be asserted that Cases 3 and 4 correspond to the best and worst "unity Courant number" schemes, respectively. All other combinations of (α, β) pairs exhibit isotropy and dispersion characteristics within the performance bounds defined by Cases 3 and 4.

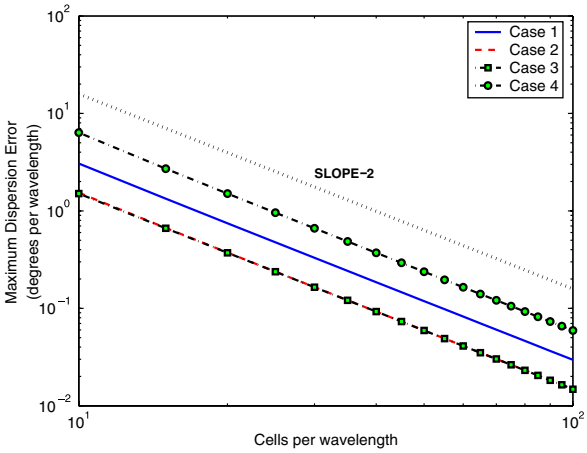

Fig. 6. Maximum dispersion error.

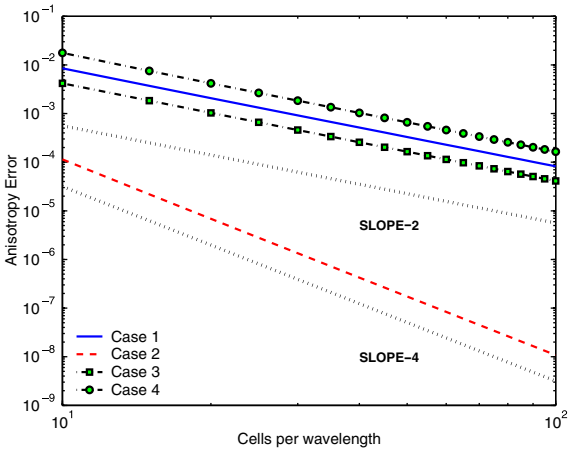

Fig. 7. Anisotropy error.

In Fig. 7 the anisotropy error for each case is plotted as a function of resolution N_λ. We have chosen to define the anisotropy error as the difference between the maximum and minimum value of $\tilde{v}_\mathrm{p}$, relative to the speed of light c. It can be seen that as (27) predicts, the Case 2 scheme exhibits fourth order anisotropy error, in contrast to the other three schemes, which are second order isotropic.

Now, let us further examine the behavior of the "unity Courant number" schemes for different values of the (α,β) pair, that lie on the CD section of Fig. 3. The analysis in the last paragraph of the previous section revealed that an equivalent expression for the update equation of $H_z\left(i+\frac{1}{2},j+\frac{1}{2}\right)$ is given in the following form:

$$\delta_t H_z\big|_{i+\frac{1}{2},j+\frac{1}{2}}^{n+1}=\frac{1}{\mu}\left[(\alpha-2\beta)(\nabla\times\mathbf{E})_z^{\text{Yee}}+4\beta(\nabla\times\mathbf{E})_z^{\text{rot-Yee}}\right]_{i+\frac{1}{2},j+\frac{1}{2}}^{n+1} \tag{38}$$

Apparently, this is a linear combination of two flux terms: one defined on a regular FDTD grid, and a second one defined on a $\pi/4$-rotated version. These are denoted as $(\nabla\times\mathbf{E})_z^{\text{Yee}}$ and $(\nabla\times\mathbf{E})_z^{\text{rot-Yee}}$, respectively. Hence, at point D we have $\alpha-2\beta=4\beta=\frac{1}{2}$. This condition indicates that the two flux terms in (38) contribute equally. However, as we move from D to C, or equivalently as $\alpha\to 2\beta$, the Yee flux term gradually vanishes, while the other term increases. In the limit, at point C, the flux is due entirely to the rhombic-cell grid arrangement. This scheme, based solely on a $\pi/4$-rotated square cell, has been shown to be equivalent to a finite-difference scheme developed on a staggered collocated grid [34,35]. The detrimental characteristic of the latter is that when excited by localised sources, it suffers from grid decoupling [8,34]. Consequently, from the "unity Courant number" schemes, the choice of $(\alpha,\beta)\equiv(3/4,1/8)$ is optimal, not only because it renders the most isotropic and the least dispersive scheme, but in addition because it prevents the development of the non-physical grid-decoupling effect.

7. Conservation properties of the extended-curl scheme

Some interesting conclusions, regarding the scheme's charge conservation properties, can be drawn from the numerical dispersion matrix shown in (25). The following approach was initially implemented by Celuch-Marcysiak and Gwarek in [36]. Hence, from the first two equations we have

$$\left.\begin{aligned}S_t\widehat{E}_x^0-\xi_y S_y\widehat{H}_z^0=0\\ S_t\widehat{E}_y^0+\xi_x S_x\widehat{H}_z^0=0\end{aligned}\right\}\Rightarrow\begin{aligned}S_t\xi_x S_x\widehat{E}_x^0-\xi_x\xi_y S_x S_y\widehat{H}_z^0=0\\ S_t\xi_y S_y\widehat{E}_y^0+\xi_x\xi_x S_x S_y\widehat{H}_z^0=0\end{aligned} \tag{39}$$

Then if we add the above two equations, we get

$$S_t\left(\xi_x S_x\widehat{E}_x^0+\xi_y S_y\widehat{E}_y^0\right)=0 \tag{40}$$

or

$$\frac{1}{\Delta t}\sin\left(\frac{\omega\Delta t}{2}\right)\left[\frac{1}{\Delta x}\sin\left(\frac{\tilde{k}_x\Delta x}{2}\right)\varepsilon\widehat{E}_x^0+\frac{1}{\Delta y}\sin\left(\frac{\tilde{k}_y\Delta y}{2}\right)\varepsilon\widehat{E}_y^0\right]=0 \tag{41}$$

Now, given the following Fourier pairs:

$$\mathcal{F}\{\delta_x\}\to-\frac{2\mathrm{j}}{\Delta x}\sin\left(\frac{\tilde{k}_x\Delta x}{2}\right)\quad\text{and}\quad\mathcal{F}\{\delta_t\}\to\frac{2\mathrm{j}}{\Delta t}\sin\left(\frac{\omega\Delta t}{2}\right) \tag{42}$$

we can conclude that (41) is the spatio-temporal Fourier transform of (15). Consequently with the aid of the numerical dispersion matrix, we have verified the conservative nature of the scheme.

Let us now examine the conservation properties of the flux-averaging scheme using the previous approach. The numerical dispersion relation in matrix form for this scheme is given by

$$\begin{bmatrix} S_t & 0 & -\xi_y S_y C_x \\ 0 & S_t & \xi_x S_x C_y \\ -\zeta_y S_y & \zeta_x S_x & S_t \end{bmatrix}\begin{bmatrix}\widehat{E}_x^0\\ \widehat{E}_y^0\\ \widehat{H}_z^0\end{bmatrix}=0 \tag{43}$$

Again, by combining the first two equations we obtain

$$\begin{aligned}&\frac{1}{\Delta t}\sin\left(\frac{\omega\Delta t}{2}\right)\left[\frac{1}{\Delta x}\sin\left(\frac{\tilde{k}_x\Delta x}{2}\right)\varepsilon\widehat{E}_x^0+\frac{1}{\Delta y}\sin\left(\frac{\tilde{k}_y\Delta y}{2}\right)\varepsilon\widehat{E}_y^0\right]\\ &\quad=\frac{2\beta}{\Delta x\Delta y}\sin\left(\frac{\tilde{k}_x\Delta x}{2}\right)\sin\left(\frac{\tilde{k}_y\Delta y}{2}\right)[\cos(\tilde{k}_x\Delta x)-\cos(\tilde{k}_y\Delta y)]\widehat{H}_z^0\end{aligned} \tag{44}$$

Obviously, the flux-averaging scheme is not conservative. From the right hand side of the above equation, we can see that the unbalanced charge is a function of both the frequency of operation as well as the propagation angle. The behavior of the residual term is better revealed by examining its Taylor expansion when $\Delta x=\Delta y=h\to 0$. It is

$$\mathrm{RHS}=\frac{\beta}{4}\tilde{k}_x\tilde{k}_y\left(-\tilde{k}_x^2+\tilde{k}_y^2\right)h^2+\mathcal{O}(h^4) \tag{45}$$

It can be seen that the excess charge is by no means negligible, and as a matter of fact it is on the order of the numerical error. This last result is an accurate quantitative measure of the artificial charge that the scheme generates, and it can be used as a criterion to determine whether the algorithm is appropriate for a given application.

It should be mentioned that an improvement in isotropy can also be achieved by the flux-averaging scheme. As a matter of fact the matrices in (25) and (43) yield the same determinant which implies that the numerical dispersion relation in (26) characterizes the flux-averaging scheme as well, or the flux-averaging scheme exhibits the same isotropy-dispersion properties. Moreover, recently Koh et al. in [37] proposed an isotropic scheme which employs a combination of an extended-curl with a flux-averaging scheme. Consequently, in terms of creating a numerical dispersion relation with improved characteristics all of the above schemes, as well those referenced in Section 1, are possible qualified candidates. However not all of them preserve the conservative nature of Maxwell's equations as characteristically demonstrated previously.

8. A higher order Laplacian realization

8.1. Formulation

In this section the extended-curl formalism is further utilized for the implementation of a higher order Laplacian (HOL) approximation. An excellent description on general HOL representations can be found in [38]. Here, we focus on Laplacian representations that utilize a 25-point stencil which are the next possible

incremental improvement over the 9-point ones. Their favorable trait is that they can be fourth order accurate, which implies that isotropic properties of sixth order should be expected. Indeed, 25-point Laplacians can exhibit isotropic phase velocity characteristics up to sixth order, and in contrast to the 9-point ones, there are more than one realizations that manifest this property [39,29]. We concentrate therefore only on isotropic 25-point Laplacians.

Given that there are multiple isotropic 25-point Laplacian stencils the main issue is to choose the best suited one for our purposes, that is for use in the FDTD update equations. Here we assume a TE_z mode and investigate the following updating scenario:

$$H_z^n \overset{\text{2-point}}{\underset{\text{curl}}{\longrightarrow}} \left\{ \begin{matrix} E_x \\ E_y \end{matrix} \right\} \overset{N\text{-point}}{\underset{\text{ext.-curl}}{\longrightarrow}} H_z^{n+1} \sim \nabla_{xy}^2 H_z^n \tag{46}$$

The primary factor that motivates which updating scenario we consider, is that the extended-curl formalism dictates that the E_x and E_y update equations remain the same as those of the Yee-scheme. For the current field mode this is realized through 2-point curl approximations, which create the following correspondences: the update of an E_x component requires the pair of the vertically placed, upper and lower H_z components. Similarly, the update of an E_y component, requires the horizontally placed, left and right H_z components. On that account, regardless of the extended-curl operator stencil, the information from the E_x and E_y components is eventually translated into vertical and horizontal H_z pairs. Consequently, one concludes that a 25-point Laplacian can be mapped into FDTD update equations, via an extended-curl operator, if its stencil can be constructed, topologically, as a combination of horizontal and vertical, possibly overlapping, H_z pairs.

After experimentation with all possible isotropic Laplacian stencils, it was concluded that the following rendition is the most straightforward to employ:

$$\nabla^2 u_{i,j} = \frac{1}{60h^2}\left(-252u_{i,j} + 52\Sigma_1 + 16\Sigma_2 - \Sigma_3 - 2\Sigma_4\right) + \frac{h^4}{90}\nabla^6 u_{i,j} + \mathcal{O}(h^6) \tag{47}$$

where the Σ terms are

$$\Sigma_1 \equiv u_{i+1,j} + u_{i-1,j} + u_{i,j+1} + u_{i,j-1} \tag{48}$$

$$\Sigma_2 \equiv u_{i+1,j+1} + u_{i+1,j-1} + u_{i-1,j-1} + u_{i-1,j+1} \tag{49}$$

$$\Sigma_3 \equiv u_{i+2,j} + u_{i-2,j} + u_{i,j+2} + u_{i,j-2} \tag{50}$$

$$\Sigma_4 \equiv u_{i+2,j+1} + u_{i+1,j+2} + u_{i-2,j+1} + u_{i-1,j+2} \tag{51}$$

$$+ u_{i-2,j-1} + u_{i-1,j-2} + u_{i+2,j-1} + u_{i+1,j-2} \tag{52}$$

and correspond to groups of points that exhibit the same $\pi/2$ rotation symmetry. One notices that the above approximation exhibits fourth order accuracy in space, and its LET is the triharmonic operator. This essentially signifies isotropic phase velocity up to sixth order.

Finally, what needs to be determined is the stencil of the extended-curl operator. The latter needs to be compatible with both the stencil of the Laplacian under study, and the Yee algorithm updating of E_x and E_y. Bearing this in mind, it can be easily verified that the spatial operator shown in Fig. 8(a) complies with both conditions. It is noticed that this is both a longitudinal and a transverse curl extension, as opposed to the transversely extended only one, presented in Section 3. The corresponding equation can be written as shown in (53)

$$\begin{aligned}\delta_t H_z\big|_{i+\frac{1}{2},j+\frac{1}{2}}^{n+\frac{1}{2}} = {} & \frac{1}{\mu}\left[B\left(\delta_y E_x\big|_{i+\frac{3}{2},j+\frac{1}{2}}^{n+\frac{1}{2}} - \delta_x E_y\big|_{i+1\frac{1}{2},j+\frac{3}{2}}^{n+\frac{1}{2}}\right) + A\left(\delta_y E_x\big|_{i+1\frac{1}{2},j+\frac{1}{2}}^{n+\frac{1}{2}} - \delta_x E_y\big|_{i+\frac{1}{2},j+1\frac{1}{2}}^{n+\frac{1}{2}}\right) + B\left(\delta_y E_x\big|_{i-\frac{1}{2},j+1\frac{1}{2}}^{n+\frac{1}{2}} - \delta_x E_y\big|_{i+\frac{1}{2},j-\frac{1}{2}}^{n+\frac{1}{2}}\right)\right] \\ & - \frac{1}{\mu}\left[D\left(\tilde{\delta}_y E_x\big|_{i+\frac{3}{2},j+\frac{1}{2}}^{n+\frac{1}{2}} - \tilde{\delta}_x E_y\big|_{i+\frac{1}{2},j+\frac{3}{2}}^{n+\frac{1}{2}}\right) + C\left(\tilde{\delta}_y E_x\big|_{i+\frac{1}{2},j+\frac{1}{2}}^{n+\frac{1}{2}} - \tilde{\delta}_x E_y\big|_{i+\frac{1}{2},j+\frac{1}{2}}^{n+\frac{1}{2}}\right)\right. \\ & \left. + D\left(\tilde{\delta}_y E_x\big|_{i-\frac{1}{2},j+\frac{1}{2}}^{n+\frac{1}{2}} - \tilde{\delta}_x E_y\big|_{i+\frac{1}{2},j-\frac{1}{2}}^{n+\frac{1}{2}}\right)\right]\end{aligned} \tag{53}$$

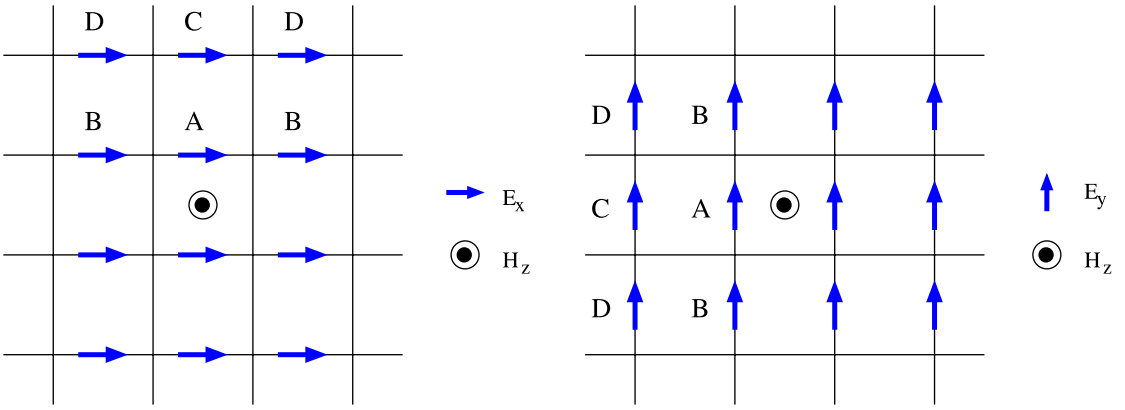

(a) Approximation of $\partial_x E_y$. (b) Approximation of $\partial_x E_y$.

Fig. 8. Higher order extended-curl discretization. Due to symmetry only half of the weights are denoted.

where

$$\tilde{\delta}_x u_i = \frac{u_{i+\frac{3}{2}} - u_{i-\frac{3}{2}}}{\Delta x} \tag{54}$$

The weights A, B, C and D are determined following a procedure analogous to that presented in Section 3. Hence, by applying Eqs. (7), (8) and (53) during a time-step cycle, one can confirm that the resulting Laplacian approximation is given by

$$\nabla^2 u_{i,j} \approx \frac{1}{h^2}[-4Au_{i,j} + (A - 2B + C)\Sigma_1 + (2B + 2D)\Sigma_2 - C\Sigma_3 - D\Sigma_4] \tag{55}$$

Then by equating like terms between the above equation and (55), we get a system of equations which solution yields $A = \frac{63}{60}$, $B = \frac{6}{60}$, $C = \frac{1}{60}$ and $D = \frac{2}{60}$. Eqs. (7), (8) and (53) constitute what we refer to as the HOL-based scheme. A general remark should be made here that for the reasons described in Section 3 we have ensured that this HOL-based scheme is consistent with both of Gauss' laws. Moreover, the HOL-based scheme cannot be realized in 3-D. However since 2-D analysis is a useful tool in electromagnetics for many important problems, it is still of great interest to examine the possibility of obtaining hyper-isotropic FDTD formulations in 2-D.

8.2. Dispersion and stability analysis of HOL-based scheme

If we assume a plane wave solution then the numerical dispersion relation for the HOL-based scheme is found to be

$$\left[\frac{1}{c\Delta t}\sin\left(\frac{\omega\Delta t}{2}\right)\right]^2 = \left(\frac{S_x}{\Delta x}\right)^2\left[C_y^{AB} - (3 - 4S_y^2)C_x^{CD}\right] + \left(\frac{S_y}{\Delta y}\right)^2\left[C_x^{AB} - (3 - 4S_x^2)C_y^{CD}\right] \tag{56}$$

where $C_w^{AB} = A + 2B\cos(\tilde{k}_w\Delta w)$ and $C_w^{CD} = C + 2D\cos(\tilde{k}_w\Delta w)$. The features of the scheme are better revealed after Taylor-expanding the above, where we obtain

$$\left(\frac{\omega}{c}\right)^2 + \mathcal{O}(\Delta t^2) = \tilde{k}_x^2 + \tilde{k}_y^2 - \frac{1}{90}\left[\Delta x^4\tilde{k}_x^6 + \Delta y^4\tilde{k}_y^6 + 3\Delta x^2\Delta y^2\left(\tilde{k}_x^4\tilde{k}_y^2 + \tilde{k}_x^2\tilde{k}_y^4\right)\right] + \mathcal{O}(\Delta x^6) + \mathcal{O}(\Delta y^6) \tag{57}$$

Evidently, the scheme is second order accurate in time and fourth order in space. Notice however that for a uniform discretization, the LET is the triharmonic operator which ensures numerical phase velocity isotropy up to 6th order. As previously, 6th order isotropy is not maintained for a non-uniform discretization. For

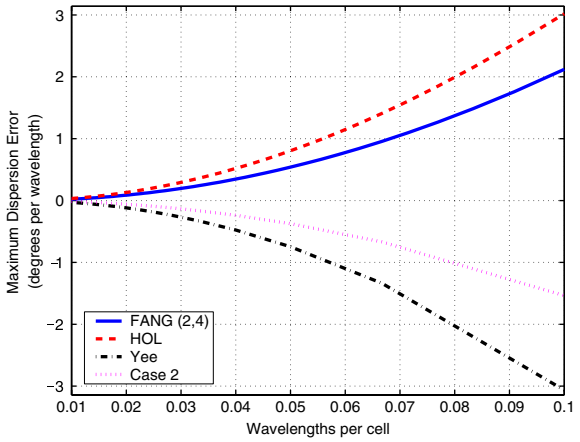

Fig. 9. Maximum algebraic dispersion error.

comparison purposes, the corresponding Taylor-expanded numerical dispersion relation for the most popular higher order FDTD scheme, namely the Fang (2, 4) scheme [1], is given by

$$\left(\frac{\omega}{c}\right)^2 + \mathcal{O}(\Delta t^2) = \tilde{k}_x^2 + \tilde{k}_y^2 - \frac{3}{320}\left(\Delta x^4 \tilde{k}_x^6 + \Delta y^4 \tilde{k}_y^6\right) + \mathcal{O}(\Delta x^6) + \mathcal{O}(\Delta y^6) \tag{58}$$

This scheme is second order accurate in time and fourth order in space; however, in contrast to (57) the LET is dependent on the propagation angle. Moreover, it is important to note that the coefficients of the two LETs, of Eqs. (57) and (58), are of the same order. This is critical because, if the coefficient of the LET in (58) was substantially less than one, the introduced anisotropy error would be insignificant, and hence the two schemes would not be comparable in absolute terms.

Furthermore, the stability limit of the HOL-based scheme can be obtained if we solve (57) with respect to the angular frequency ω and require the latter being real for all values of $\tilde{k}_x$ and $\tilde{k}_y$. Accordingly, the time-step bound that ensures stability is given by

$$\Delta t \leqslant \sqrt{\frac{10}{9}}\frac{h}{c\sqrt{2}} \tag{59}$$

Notice that for the derivation of the above condition a square cell of size h has been assumed, since for this type of grids the proposed scheme exhibits its superior characteristics. Additionally, (59) is less restrictive than the corresponding conditions, for the Yee and the Fang (2, 4) scheme (the time-step bound for the former is given by $\Delta t \leqslant \frac{h}{c\sqrt{2}}$ and for the latter by $\Delta t \leqslant \frac{6h}{7c\sqrt{2}}$).

In Fig. 9, where the algebraic[1] value of the maximum dispersion error is plotted as a function of the inverse resolution N_λ^{-1}. For all schemes the maximum stable time-step is used. It can be seen that the HOL-based scheme, as well as the Fang (2, 4) deviate positively from the zero dispersion error curve.

These curves are juxtaposed with the ones that correspond to the Yee and the Case 2 scheme, which both deviate negatively. Moreover, it should be mentioned that the latter two schemes exhibit their optimum behavior at the Courant stability limit, and in particular their dispersion error is upper bounded by the zero dispersion error curve. Nevertheless, this is not the case when it comes to the HOL-based, as well as the Fang (2, 4) scheme. More precisely by reducing the time-step or equivalently by reducing the Courant number, the temporal error can become comparable to the spatial one and even cancel each other out. At this point the dispersion error curve exhibits a zero-crossing which means that for the discretization that this occurs, superior

[1] We define the algebraic maximum dispersion error ζ as

$$|\zeta| = 360^\circ \max_{\phi}\left\{\left|1 - \frac{\tilde{v}_p}{c}\right|\right\}.$$

accuracy can be achieved. As a matter of fact, there can be an optimal Courant number which minimizes the dispersion error over all propagation angles, for a fixed resolution [16]. Its derivation requires the minimization of some appropriately chosen quantity. For example if we define as an optimization constraint the minimization of the following quantity:

$$J = \int_0^{\pi/2} \left| 1 - \frac{\tilde{v}_p}{c} \right| d\phi \tag{60}$$

Then by using a simple searching algorithm the Courant number can be determined that guarantees superior accuracy for a given N_λ.

The above optimization procedure was applied to both the HOL-based and the Fang (2,4) scheme, for a discretization of $N_\lambda = 30$. The corresponding results are shown in Fig. 10(a) and (b). As regards to the maximum dispersion error it can be seen that although both schemes exhibit the same rate of descent, the HOL-based for the optimized resolution exhibits a deep null which, apparently, indicates almost total elimination of the dispersion error. Note here that the corresponding Courant numbers are $S = 0.0763$ and $S = 0.0557$ for the HOL-based and the Fang (2,4) scheme, respectively (so these approaches are of limited usefulness for most practical cases). Additionally in Fig. 10(b) the phase velocity deviation $1 - \frac{\tilde{v}_p}{c}$, is depicted at $N_\lambda = 30$, as a function of the propagation angle. The HOL-based scheme is substantially more isotropic and from the inset figure we can see that the magnitude of its phase velocity deviation, is 10^3 times less than that of the Fang (2,4).

Finally, the scheme's performance with respect to the anisotropy error is also depicted in Fig. 11. As expected the performance of the HOL-based scheme is outstanding. From the same figure we also observe that although the Case 2 and the Fang (2,4) are both fourth order isotropic, the former introduces less anisotropy error.

In conclusion the following points should be emphasized. First of all in Fig. 9 it can be seen that the Fang (2,4) is less dispersive than the HOL-based scheme. This is attributed to the fact that the LET coefficients may be of the same order, however the Fang (2,4) one is slightly smaller, hence it is less dispersive. This is true provided that the same time integration scheme is applied, meaning that the same amount of temporal discretization error is introduced.

Furthermore it should be mentioned that comparing the HOL-based scheme to the Fang (2,4) is not absolutely "fair" in terms of Laplacian realizations. In particular, the Fang (2,4) essentially recovers the stencil of a 49-point Laplacian, therefore a "fair" comparison would be against a HOL-based scheme that utilizes an isotropic 49-point Laplacian stencil. Nonetheless, it was demonstrated that just a 25-point Laplacian realization is sufficient to create an FDTD scheme with performance comparable to that of the Fang (2,4), which clearly indicates that the extended-curl scheme achieves a more efficient stencil utilization. Finally, in Table 2 there is a comparison of the actual computational burden of the schemes under study. It can be seen that the extended-curl and

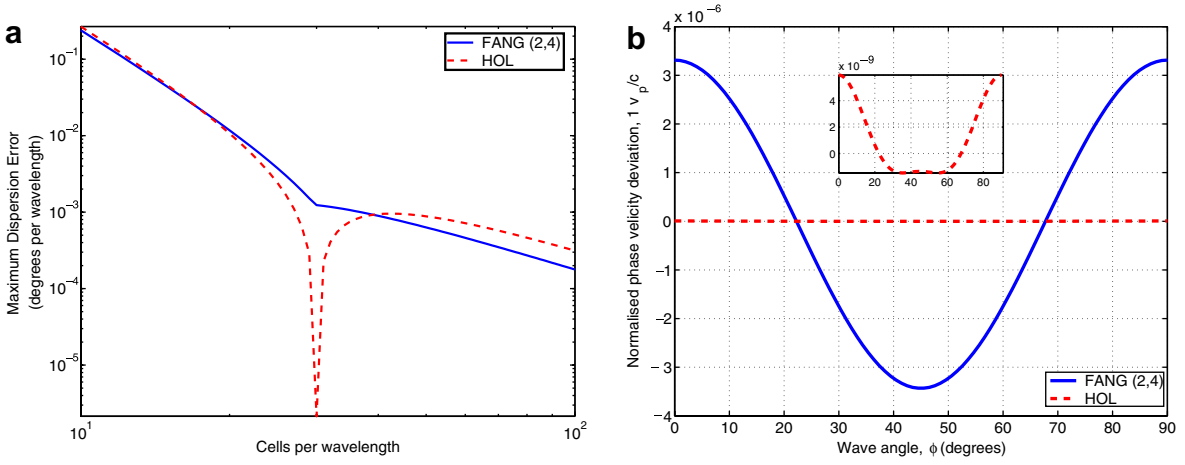

Fig. 10. (a) Maximum dispersion error. (b) Phase velocity deviation. Optimization at $N_\lambda = 30$.

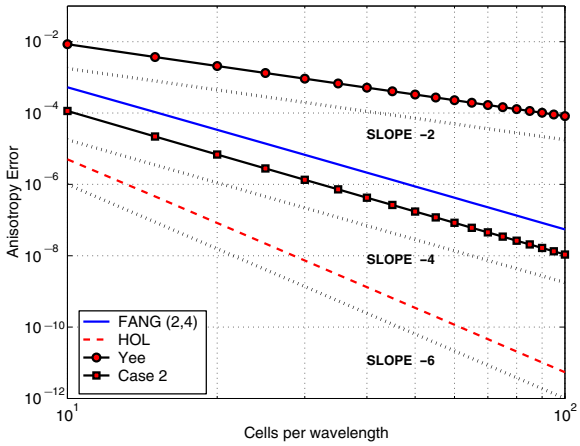

Fig. 11. Anisotropy error.

Table 2
Comparison of computational load

	Yee	Extended curl	Fang (2,4)	HOL
FLOPS	11	20	22	34

the HOL-based scheme are computationally more expensive than the Yee and the Fang scheme, respectively. For completeness we mention that in 3-D the extended-curl scheme requires 16 flops, while the Yee algorithm requires 5 flops, per component update.

9. Numerical experiments

9.1. Radiation pattern

In this example we calculate the radiation pattern of two infinite line sources. The sources extend to infinity along the z-axis, they are located symmetrically with respect to the origin along the y-axis, and they are uniformly excited. Given that the distance between the two sources is d then the total magnetic field at a distance ρ in the far-field is given by

$$\mathbf{H} = -\widehat{a}_z \frac{I_m}{\eta}\sqrt{\frac{\mathrm{j}\beta}{8\pi}}\frac{\mathrm{e}^{-\mathrm{j}\beta\rho}}{\sqrt{\rho}}\left[2\cos\left(\frac{\beta d}{2}\sin\phi\right)\right] \tag{61}$$

Notice that if we choose $\beta d/2$ to be odd multiples of $\pi/2$, then at $\phi = \pi/2$ and $\phi = 3\pi/2$ the radiation pattern of this structure exhibits nulls. Now, when trying to model this configuration in FDTD, the destructive interference between the two sources along the direction of the nulls, is not exactly predicted due to dispersion. This implies that the radiation pattern for these angles does not vanish but exhibits some finite value. Moreover, if the distance between the sources is electrically large, in the direction of the nulls the radiation pattern exhibits minor lobes whose maximum values can be comparable to that of the actual pattern.

The above scenario was modeled using both the Yee algorithm as well as the Case 2 scheme. A relatively coarse discretization of $\lambda/6$ was chosen, and two different distances from the source were examined, namely 2.5λ and 5.5λ. The excitation of the domain is realized by imposing a soft source condition on the appropriate H_z components. Since this is a single frequency problem we can take advantage of the isotropic properties of the Case 2 numerical velocity, and so we optimized it with respect to the dispersion error at the particular discretization of interest. This was achieved by setting the numerical wavenumber equal to its exact value along some direction. This can be realized by appropriately scaling the free space material properties. The adjustment was made with respect to the wavenumber along the $\phi = 45°$ direction, given by

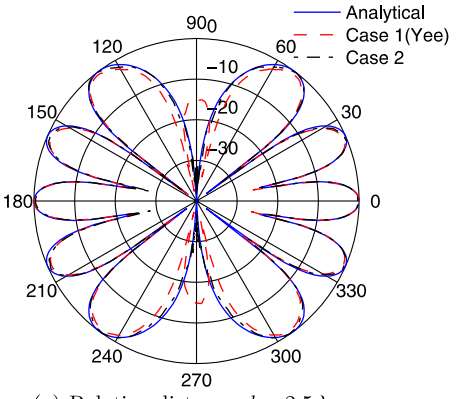

(a) Relative distance $d = 2.5\,\lambda$.

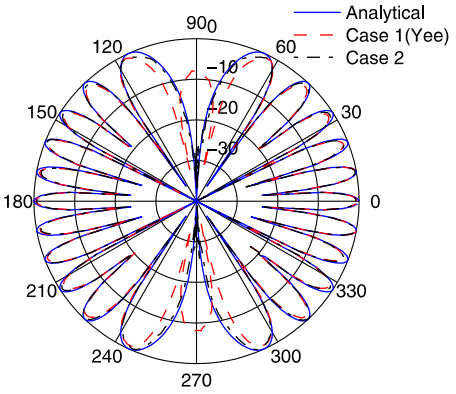

(b) Relative distance $d = 5.5\,\lambda$.

Fig. 12. Radiation pattern predictions of two infinite current sources uniformly excited. Discretization $h = \lambda/6$.

$$\tilde{k} = \frac{2\sqrt{2}}{h}\arcsin\sqrt{\frac{1-\sqrt{1-16\beta\left[\frac{1}{S\sqrt{2}}\sin\left(\frac{\pi S}{N_\lambda}\right)\right]}}{8\beta}} \tag{62}$$

The corresponding radiation patterns are shown in Fig. 12(a) and (b). It can be seen that along $\phi = \pi/2$ and $\phi = 3\pi/2$ the Yee-scheme exhibits a spurious minor lobe while the Case 2 scheme does not.

9.2. Waveguide propagation constant

In this example a parallel plate waveguide is modeled. The TE_z mode is excited by injecting a z-directed magnetic field, with a very sharp differentiated Gaussian pulse time dependence. The dimensions of the waveguide are 13 by 40 cells, and the cell size is set equal to $h = 1$ cm. The propagation constant information is extracted using the following procedure. The time-history of the electric field component E_x is observed along two transverse planes separated by a distance $d = h$. The first observation plane is located 10 cells away from the excitation point. Then, the observed quantities are Fourier transformed, and the information for each excited mode is obtained by utilizing the orthogonality properties of the field eigenfunctions, that is

$$E_x = -\frac{\mathrm{j}\beta}{k_c}A_n\cos\left(\frac{n\pi x}{d}\right)\mathrm{e}^{-\mathrm{j}\beta y} \Rightarrow \int_0^d E_x\cos\left(\frac{m\pi x}{d}\right)\mathrm{d}x = -\frac{\mathrm{j}\beta}{k_c}A_n\pi\delta_{mn}\mathrm{e}^{-\mathrm{j}\beta y} \tag{63}$$

Then, we divide the integrated quantities for the two observation planes and the ratio is equal to $\mathrm{e}^{-\mathrm{j}\beta d}$, and hence the values of β can be easily extracted. The propagation constant of the first eight modes is computed using the Yee, the Case 3, the Fang, and the HOL scheme. The corresponding results are shown in Fig. 13(a)–(d). First, it

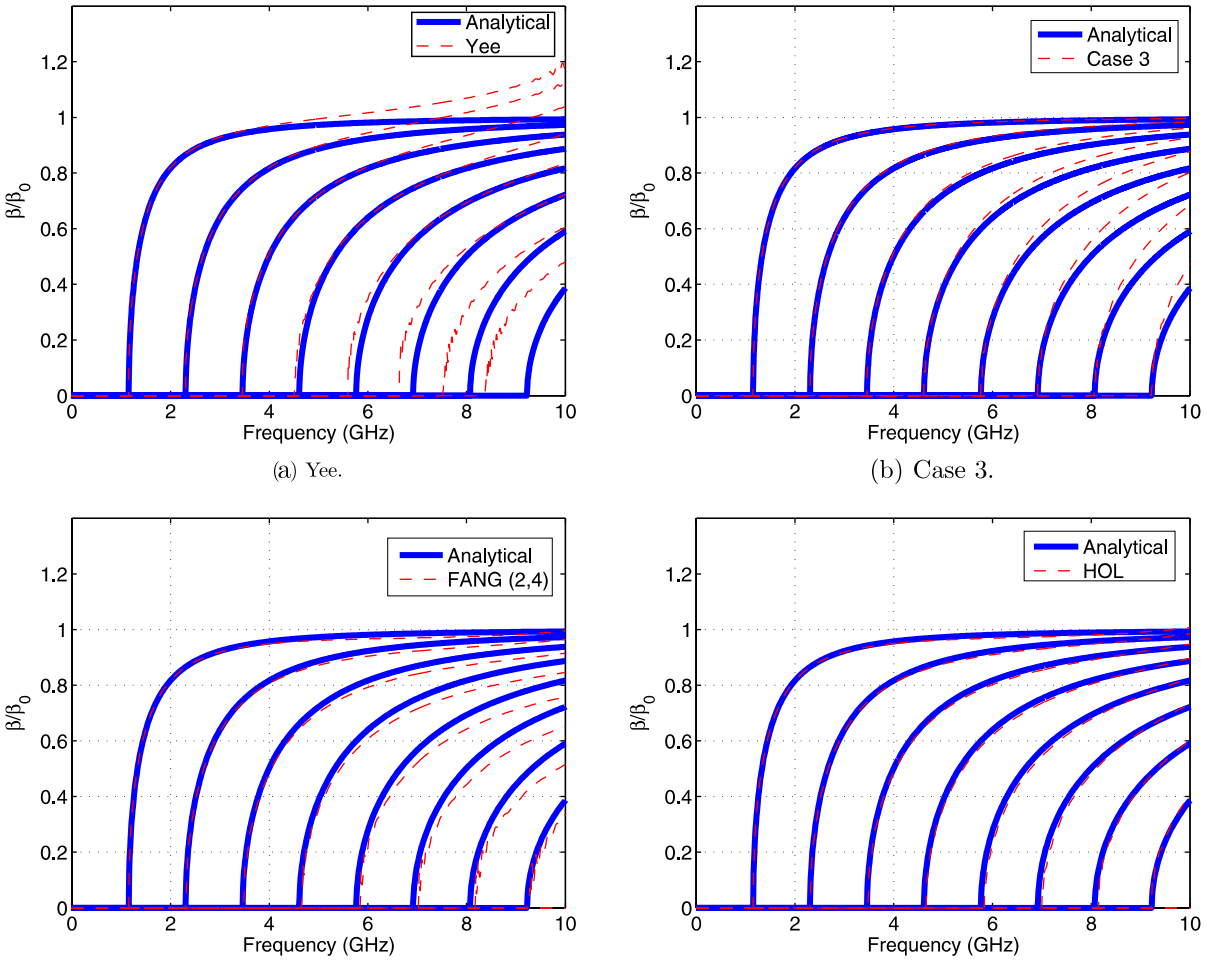

(a) Yee. (b) Case 3.

(c) Fang (2,4). (d) HOL.

Fig. 13. Normalized propagation constant β/β_0 versus frequency.

can be seen that the results corresponding to the Case 3 are in better agreement to the theoretical expected ones than are the results obtained by the Yee-scheme. It is interesting to note that the Case 3 scheme predicts very accurately the cut-off frequencies. This is a direct consequence of the fact that at cut-off the waves essentially propagate along the $\phi = 90°$ direction where the scheme is dispersionless.

Second, it can be seen that the HOL-based scheme outperforms the Fang scheme. However, on purpose, for this set of simulations both schemes were operated at the Courant limit of the Fang scheme, that is $S = \frac{6h}{7c\sqrt{2}}$. This is because from our experimentation with the dispersion error curves it was found that the HOL-based scheme, for the above Courant number, exhibits the same dispersion characteristics as the Fang scheme down to 10 cells per wavelength. But from 3 to 10 cells per wavelength it becomes slightly less dispersive. Indeed, from Fig. 13(c) and (d) we can seen that up to 3 GHz ($\lambda/10$) both schemes exhibit the same performance. However, from 3 GHz to 10 GHz ($\lambda/10$ to $\lambda/3$) the HOL-based scheme is in better agreement to the analytical results. Obviously, if both schemes were operated at their Courant limit, the Fang scheme would yield better results.

Also, for the modeling of the PEC plates image theory was used. In this case the image principle is easy to apply due to the simplicity of the geometry (infinite in extent). However, for a continuously varying PEC boundary the implementation of the image principle is not straightforward and it can be a very laborious programming exercise. In these cases, our experimentation revealed that the elementary PEC object where image

Fig. 14. (a, b) Scattering by a dielectric coate h, $h = \lambda/20$. (c, Scattering d) Scat $= 20h$ h $\rho = 20h$, $h = \lambda/20$.

theory is applicable, and yields stable simulations, is a sequence of 3 PEC patches (all four cell edges made out of PEC). For such an object image theory should be applied only for the PEC patch in the middle.

9.3. Scattering width

In the last example we examine the scattering by infinite (along the z-direction) cylinders of circular cross-section. Three different cylinders were examined: a dielectric, a PEC and a dielectric coated PEC cylinder. The first two have a radius of 20 cells. The third one consists of a 15 cell PEC core coated by a 5-cell dielectric shell. For the first and third cylinder the dielectric material has a permittivity of $\varepsilon_r = 2$. The cell size for all simulations is set equal to $\lambda/20$. All scatterers are illuminated by a TE_z uniform plane wave. In Fig. 14(a), (c) and (e) there are the scattering width predictions as provided by the Yee and the Case 2 scheme along with the analytical solution. It can be seen that both schemes exhibit the same accuracy and they are in good agreement with the analytical solution. Additionally, in Fig. 14(b), (d) and (f) there is the time-domain response of the scattered field along the backscattered direction. The observation point is located 40 cells away from the center of the cylinder. Similarly, it can be seen that the Yee and the Case 2 scheme are in excellent agreement. It needs to be mentioned that for this set of experiments the PEC objects were created using PEC patches. Furthermore, for the Case 2 simulations no special treatment was performed along the material boundaries.

10. Conclusions

We have described a general framework for the design of stable FDTD schemes based on improved approximations of the transverse Laplacian term associated with the curl–curl operator. Depending on the Laplacian approximation the resulting scheme can be more isotropic, less dispersive and have a higher Courant number than the conventional Yee algorithm and many of its improvements found in the literature. As a matter of fact, it was proved that this family of schemes can support a unity Courant number without the corresponding scheme suffering from grid decoupling.

Representative numerical experiments were performed that verified the theoretically expected behavior. Furthermore, it was found that due to the extended stencil of the proposed schemes, their performance is strongly dependent on the accurate modeling of inhomogeneities. For cases where the above is feasible the proposed schemes yield more accurate results. In any other case, their improved dispersion and anisotropy characteristics are masked by the errors introduced by the material modeling inaccuracies.

Acknowledgement

This project was funded by DARPA. The authors would like to thank Dr. Ben Mann, DARPA-DSO, and Dr. Reza Malek-Madani, ONR, for their continued interest and support of this project.

Appendix A

In this section we derive the maximum value of the following quantity:

$$J = \sin^2\left(\frac{x}{2}\right)\left[\alpha + 2\beta\cos(y)\right] + \sin^2\left(\frac{y}{2}\right)\left[\alpha + 2\beta\cos(x)\right] \tag{A.1}$$

given that $\alpha + 2\beta = 1$. For simplicity we set

$$\sin^2\left(\frac{x}{2}\right) \equiv x \quad \text{and} \quad \sin^2\left(\frac{y}{2}\right) \equiv y$$

therefore

$$J = x(1 - 4\beta y) + y(1 - 4\beta x) \tag{A.2}$$

with $x, y \in [0, 1]$. It is

$$J = (A - 4\beta B)x + B \tag{A.3}$$

where

$$A \equiv 1 - 4\beta y \quad \text{and} \quad B \equiv y$$

We examine the following cases:

(1) $A - 4\beta B > 0$
Then J is monotonically increasing, therefore

$$J_{\max} = J(x = 1) = A + (1 - 4\beta)B = 1 + (1 - 8\beta)y$$

and

(a) if $1 - 8\beta > 0$ then $J_{\max} = J(x = 1; y = 1) = 2 - 8\beta$;
(b) if $1 - 8\beta \leqslant 0$ then $J_{\max} = J(x = 1; y = 0) = 1$.

(2) $A - 4\beta B \leqslant 0$
Then J is monotonically decreasing, therefore

$$J_{\max} = J(x = 0) = B = y$$

and obviously

$$J_{\max} = J(x = 0;\ y = 1) = 1$$

We can conclude that

$$J_{\max} = \max_{\beta}\{1, 2 - 8\beta\}, \quad \forall \beta \in \mathbb{R} \tag{A.4}$$

References

[1] J. Fang, Time domain finite difference computation for Maxwell's equations, Ph.D. thesis, University of California at Berkeley, Berkeley, CA, 1989.
[2] A. Yefet, P.G. Petropoulos, A staggered fourth-order accurate explicit finite difference scheme for the time-domain Maxwell's equations, J. Comput. Phys. 168 (2) (2001) 286–315.
[3] T.T. Zygiridis, T.D. Tsiboukis, Low-dispersion algorithms based on the higher order (2,4) FDTD method, IEEE Trans. Microwave Theory Tech. 52 (4) (2004) 1321–1327.
[4] G. Sun, C.W. Trueman, Optimized finite-difference time-domain methods based on the (2,4) stencil, IEEE Trans. Microwave Theory Tech. 53 (3) (2005) 832–842.
[5] M.F. Hadi, M. Piket-May, A modified FDTD (2,4) scheme for modeling electrically large structures with high-phase accuracy, IEEE Trans. Antennas Propagat. 45 (2) (1997) 254–264.
[6] J.L. Young, D. Gaitonde, J.S. Shang, Toward the construction of a fourth-order difference scheme for transient EM wave simulation: staggered grid approach, IEEE Trans. Antennas Propagat. 45 (11) (1997) 1573–1580.
[7] S.K. Lele, Compact finite difference schemes with spectral resolution, J. Comput. Phys. 101 (1992) 16–42.
[8] Y. Liu, Fourier analysis of numerical algorithms for the Maxwell equations, J. Comput. Phys. 124 (1996) 396–416.
[9] F. Xiao, X. Tang, X. Zhang, The construction of low-dispersive FDTD on hexagon, IEEE Trans. Antennas Propagat. 53 (11) (2005) 3697–3703.
[10] J.S. Juntunen, T.D. Tsiboukis, Reduction of numerical dispersion in FDTD method through artificial anisotropy, IEEE Trans. Microwave Theory Tech. 48 (4) (2000) 582–588.
[11] S. Wang, F.L. Teixeira, A finite-difference time-domain algorithm optimized for arbitrary propagation angles, IEEE Trans. Antennas Propagat. 51 (9) (2003) 2456–2463.
[12] S. Wang, F.L. Teixeira, Dispersion-relation-preserving FDTD algorithms for large-scale three-dimensional problems, IEEE Trans. Antennas Propagat. 51 (8) (2003) 1818–1828.
[13] S. Wang, F.L. Teixeira, A three-dimensional angle-optimized finite-difference time-domain algorithm, IEEE Trans. Microwave Theory Tech. 51 (3) (2003) 811–817.
[14] S. Wang, F.L. Teixeira, Grid-dispersion error reduction for broadband FDTD electromagnetic simulations, IEEE Trans. Magn. 40 (2) (2004) 1440–1443.
[15] S. Wang, F.L. Teixeira, Lattice models for large-scale simulations of coherent wave scattering, Phys. Rev. E 69 (2004).
[16] K.L. Shlager, J.B. Schneider, Comparison of the dispersion properties of several low-dispersion finite-difference time-domain algorithms, IEEE Trans. Antennas Propagat. 51 (3) (2003) 642–653.

[17] B. Finkelstein, R. Kastner, Finite difference time domain dispersion reduction schemes, J. Comput. Phys. 221 (1) (2007) 422–438.
[18] Q.H. Liu, The PSTD algorithm: a time-domain method requiring only two cells per wavelength, Microwave Opt. Technol. Lett. 15 (3) (1997) 158–165.
[19] Q.H. Liu, Large-scale simulations of electromagnetic and acoustic measurements using the pseudospectral time-domain (PSTD) algorithm, IEEE Trans. Geosci. Remote Sens. 37 (2) (1999) 917–926.
[20] Q.H. Liu, G. Zhao, Review of PSTD methods for transient electromagnetics, Int. J. Numer. Model. 17 (3) (2004) 99–323.
[21] J.S. Hesthaven, High-order accurate methods in time-domain computational electromagnetics: a review, Adv. Imag. Elect. Phys. 127 (2003) 59–123.
[22] N.V. Kantartzis, T.D. Tsiboukis, Higher-order FDTD Schemes for Waveguide and Antenna Structures, Morgan & Claypool, San Rafel, CA, 2006.
[23] N.V. Kantartzis, T.D. Tsiboukis, A higher order nonstandard FDTD-PML method for the advanced modeling of complex EMC problems in generalized 3-D curvilinear coordinates, IEEE Trans. Electromagn. Compat. 46 (1) (2004) 2–11.
[24] N.V. Kantartzis, T.D. Tsiboukis, A generalized methodology based on higher-order conventional and non-standard FDTD concepts for the systematic development of enhanced dispersionless wide-angle absorbing perfectly matched layers, Int. J. Numer. Model. 13 (5) (2000) 417–440.
[25] A.H. Panaretos, J.T. Aberle, R.E. Díaz, A three-dimensional finite-difference time-domain scheme based on a transversely extended curl operator, IEEE Trans. Microwave Theory Tech. 54 (12) (2006) 4237–4246.
[26] K.S. Yee, Numerical solution of initial boundary value problems involving Maxwell's equations in isotropic media, IEEE Trans. Antennas Propagat. 14 (8) (1966) 302–307.
[27] A.T. Taflove, S.C. Hagness, Computational Electrodynamics: The Finite-Difference Time-Domain Method, second ed., Artech House, 2000.
[28] K.S. Kunz, R.J. Luebbers, The Finite Difference Time Domain Method for Electromagnetics, CRC Press, 1993.
[29] M. Patra, M. Karttunen, Stencils with isotropic discretization error for differential operators, Numer. Methods Part. Diff. Equ. 22 (4) (2006) 936–953.
[30] G.H. Cohen, Higher-order Numerical Methods for Transient Wave Equations, Springer, 2002.
[31] E.A. Forgy, A time-domain method for computational electromagnetics with isotropic numerical dispersion on an overlapped lattice, Master's thesis, University of Illinois at Urbana, Champaign, 1998.
[32] Z. Bi, K. Wu, C. Wu, J. Litva, A new finite-difference time-domain algorithm for solving Maxwell's equations, IEEE Microwave Guided Wave Lett. 1 (12) (1991) 382–384.
[33] M.S. Min, C.H. Teng, The instability of the Yee scheme for the magic time step, J. Comput. Phys. 166 (2001) 418–424.
[34] S.L. Ray, Grid decoupling in finite element solutions of Maxwell's equations, IEEE Trans. Antennas Propagat. 40 (4) (1992) 443–445.
[35] E.A. Forgy, W.C. Chew, A time-domain method with isotropic dispersion and increased stability on an overlapped lattice, IEEE Trans. Antennas Propagat. 50 (7) (2002) 983–996.
[36] M. Celuch-Marcysiak, W.K. Gwarek, On the nature of solutions produced by finite difference schemes in the time domain, Int. J. Numer. Model. 12 (1999) 23–40.
[37] I.S. Koh, H. Kim, J.M. Lee, J.G. Yook, C.S. Pil, Novel explicit 2-D FDTD scheme with isotropic dispersion and enhanced stability, IEEE Trans. Antennas Propagat. 54 (11) (2006) 3505–3510.
[38] L. Collatz, The Numerical Treatment of Differential Equations, third ed., Springer-Verlag, 1966.
[39] G. Cohen, A class of schemes, fourth order in space and time, for the 2D wave equation, in: Proceedings of the Sixth IMACS Intenational Symposium on Computer Methods for Partial Differential Equations, Bethlehem, PA, USA, 1987, pp. 23–27.